Surface-Wave Dispersion in Partially Saturated Soils: The Role of Capillary Forces

Santiago G Solazzi, Ludovic Bodet, Klaus Holliger, Damien Jougnot

JGR Solid Earth

RESEARCH ARTICLE
10.1029/2021JB022074

Surface-Wave Dispersion in Partially Saturated Soils: The Role of Capillary Forces

Santiago G. Solazzi[1], Ludovic Bodet[2], Klaus Holliger[1], and Damien Jougnot[2]

[1]Institute of Earth Sciences, University of Lausanne, Lausanne, Switzerland, [2]Sorbonne Université, CNRS, EPHE, Paris, France

Key Points:

- Water content variations in the partially saturated zone hardly alter V_p/V_s ratios, but have large effects on surface-wave signatures
- The effective soil stress is strongly affected by capillary forces, which stiffen the medium at relatively low saturations
- Capillary effects permit to explain observed changes in surface-wave dispersion due to small water content variations in the vadose zone

Correspondence to:
S. G. Solazzi,
Santiago.Solazzi@unil.ch

Citation:
Solazzi, S. G., Bodet, L., Holliger, K., & Jougnot, D. (2021). Surface-wave dispersion in partially saturated soils: The role of capillary forces. *Journal of Geophysical Research: Solid Earth*, *126*, e2021JB022074. https://doi.org/10.1029/2021JB022074

Received 15 MAR 2021
Accepted 6 NOV 2021

Author Contributions:

Conceptualization: Santiago G. Solazzi, Ludovic Bodet, Klaus Holliger, Damien Jougnot
Formal analysis: Santiago G. Solazzi, Ludovic Bodet
Investigation: Ludovic Bodet, Klaus Holliger, Damien Jougnot
Methodology: Santiago G. Solazzi
Visualization: Santiago G. Solazzi, Ludovic Bodet, Damien Jougnot
Writing – original draft: Santiago G. Solazzi, Ludovic Bodet
Writing – review & editing: Santiago G. Solazzi, Ludovic Bodet, Klaus Holliger, Damien Jougnot

Abstract Improving our understanding of the relation between the water content and the seismic signatures of unconsolidated superficial soils is an important objective in the overall field of hydrogeophysics. Current approaches to constrain the water content in the vadose zone from seismic data are based on computing the ratio between compressional and shear wave velocities V_p/V_s. While this allows for the detection of pronounced changes in saturation, such as the groundwater table, it is essentially insensitive to variations in the saturation-depth profile. Conversely, evidence shows that surface waves are sensitive to both the location of the water table and the saturation-depth profile. Classic rock physics models are unable to explain the corresponding observations. We propose to estimate surface-wave signatures accounting for capillary suction effects. We extend the Hertz-Mindlin model using Bishop's effective stress definition, thus accounting for stiffness changes associated with capillary stresses acting on the soil's frame. We then compute the elastic properties of the partially saturated medium using the Biot-Gassmann-Wood model. Considering a 1D unconsolidated porous medium under steady-state saturation conditions, as given by Richards' equation, we simulate body-wave travel times and surface-wave dispersion characteristics for different water table depths and overlying soil textures. Our results illustrate that surface-wave phase velocity dispersion curves are remarkably sensitive to capillary effects in partially saturated soils, exhibiting velocity changes of up to 20% in the 10–100 Hz frequency range. These effects, which are particularly important in medium-to fine-grained soils, are virtually nonexistent in the corresponding V_p/V_s profiles.

Plain Language Summary Seismic waves are usually employed to study the water content in the shallow subsurface for environmental purposes. Most studies estimate the water content of the soil at different depths relating compressional and shear wave velocities, which are estimated by measuring body-wave travel times. Even though this method permits to locate the depth at which the soil becomes fully water saturated, it is rather insensitive to changes in the water content of the overlaying portion of the soil, where partial air-water saturation prevails. Surface waves, however, appear to be significantly sensitive to changes in saturation within this partially saturated region. Classic rock physics models cannot explain this difference in sensitivity between surface-wave velocity and body-wave travel times. In this work, we propose to include the effects of capillary forces, which arise when the soil is partially saturated, in the rock physics models. By doing so, we show that capillary action, which acts bringing soil particles further together, can explain why surface-wave dispersion curves are sensitive to saturation variations in the partially saturated zone while body-wave travel times remain virtually unperturbed. These results may help to better interpret seismic data for environmental studies.

1. Introduction

The critical zone is a region of the shallow subsurface that ranges from the top of the vegetation canopy to the base of superficial aquifers. It comprises rocks, soils, water, air, and living organisms; contains the vast majority of life-sustaining resources; and regulates the interaction between the atmosphere and aquifers (e.g., Binley et al., 2015; Parsekian et al., 2015). The combined use of geophysical multiscale probing and imaging techniques along with the integration of hydrological, hydrogeological, and geochemical data is widely practiced for the observation of the partially saturated region of the critical zone, that is, the vadose zone (e.g., Parsekian et al., 2015). This approach to geophysical subsurface characterization, referred to as hydrogeophysics (e.g., Hubbard & Linde, 2011; Rubin & Hubbard, 2006), is dominated by electrical and electromagnetic methods due to their strong sensitivity with regard to water content and salinity (e.g., Friedman, 2005). However, given that seismic waves are inherently sensitive to key hydraulic properties of porous media, such as, porosity, permeability,

and saturation, seismic techniques have the potential to provide valuable complementary information (e.g., Bradford & Sawyer, 2002; Milani et al., 2015; Pride, 2005; Rubin & Hubbard, 2006).

In near-surface applications, P- and S-wave seismic velocities, denoted as V_p and V_s, respectively, can be estimated through refraction tomography, that is, by analyzing corresponding travel times (e.g., Grelle & Guadagno, 2009; Turesson, 2007). In order to avoid difficulties associated with additional horizontal geophone setups and S-wave sources, V_s characteristics tend to be inferred through the analysis of surface-wave dispersion (e.g., Foti et al., 2018; Socco & Strobbia, 2004). The combination of refraction tomography and surface-wave dispersion analysis, enabling the "simultaneous" estimation of 2D V_p and V_s sections along coincident profiles, has been extensively developed in recent studies (e.g., Konstantaki et al., 2013; Pasquet, Bodet, Dhemaied, et al., 2015; Pasquet, Bodet, Longuevergne, et al., 2015; Pasquet & Bodet, 2017). In this context, V_p/V_s or equivalently, Poisson's ratios can be estimated and interpreted to delineate the transition between partially saturated (low V_p/V_s ratios) and fully saturated soils (high V_p/V_s ratios) (e.g., Konstantaki et al., 2013; Pasquet, Bodet, Dhemaied, et al., 2015; Pasquet, Bodet, Longuevergne, et al., 2015). Although this approach enables the distinction between unsaturated and saturated regions in the shallow subsurface, it inherently suffers from two main drawbacks (Bodet, 2019): (a) Current inversion techniques are limited to a relatively small number of layers that cannot adequately describe the continuous variations of the saturation comprised between the water table and the surface; (b) interpretations are frequently restricted to a binary estimation of saturation, that is, partially versus fully saturated, based on the V_p/V_s values and hence, do not allow for a detailed assessment of the soil water characteristics. Correspondingly, the use of Poisson's ratios or V_p/V_s estimates for estimating saturation profiles remains largely limited to studies with strong complementary information from borehole logs, geotechnics, hydrogeology, and alternative geophysical characterizations (e.g., Pasquet, Holbrook, et al., 2016; Pasquet & Bodet, 2017). All this points to the need for novel techniques to constrain the soil water content in the vadose zone and its evolution from seismic data.

An interesting approach is to consider that changes in the water content due to climate-related hydrological conditions occur over relatively short timescales, for which, solid frame properties of siliciclastic soils can be assumed to remain invariant (e.g., Bergamo et al., 2016a, 2016b). In this context, experimental evidence shows that local saturation changes in the vadose zone influence surface-wave dispersion data. For instance, using the ~5.5-m-length profiles with an ~2-m maximum exploration depth, Z. Lu (2014) showed that surface-wave dispersion curves are profoundly affected by seasonal variations in water content. Interestingly, differences in surface-wave dispersion at various saturation states were also observed at the centimeter scale in laboratory studies of granular media (Pasquet, Bodet, et al., 2016). The abovementioned studies, together with additional experimental evidence (e.g., Bodet, 2019; West & Menke, 2000), consistently point to the sensitivity of surface-wave dispersion with regard to saturation changes in the vadose zone. However, even under well-controlled experimental conditions, surface-wave dispersion data remain difficult to interpret based on current models (Blazevic et al., 2020). A possible reason for this is that most rock physics models have been developed to fit body-wave travel times, which, in turn, appear to be inexplicably insensitive to the water content in the partially saturated zone overlying the water table. This illustrates the need for a fundamental revision of forward models, which could enable process-based imaging and monitoring approaches, such as, for example, passive seismic interferometry for hydrogeophysical characterization (Fores et al., 2018; Lecocq et al., 2017).

The interpretation of surficial soil mechanical properties and the estimation of the corresponding hydrodynamic parameters using seismic data are complex tasks. Most related research efforts employ the Hertz-Mindlin (HM) (Mindlin, 1949) contact theory combined with the Biot-Gassmann (BG; Gassmann, 1951) model (e.g., Dvorkin et al., 1999). Consequently, the soil is conceptualized as an aggregate of spheroidal particles held together by the effective stress. In the particular case of partially saturated soils, it is commonly assumed that such a medium is saturated by an effective fluid, whose properties are given by the weighted average of the properties of the immiscible pore fluid phases (e.g., Bachrach et al., 1998; Pasquet, Holbrook, et al., 2016; Shen et al., 2016). However, contrary to the classic HM-BG model, field observations and laboratory experiments show that the effective stress is not only affected by the overburden and pore pressures, but also and in particular, by capillary forces (e.g., Cho & Santamarina, 2001; Dong & Lu, 2016; N. Lu & Likos, 2004; Santamarina et al., 2005). Since the pioneering work of Bishop and Blight (1963), several authors have explored the stiffening effects associated with capillary suction, which prevail when soil grains are pulled closer together by surface tension acting at the interfaces between immiscible pore fluid components, such as air and water, and their enclosing grain surfaces (Cho & Santamarina, 2001; Fratta et al., 2005; Shen et al., 2016). Indeed, there is evidence to suggest that, for

soils comprising small characteristic grain sizes, capillary forces may have a dominant effect on the effective elastic moduli and, thus, on V_p and V_s (e.g., Heitor et al., 2012; Sawangsuriya et al., 2009).

Previous studies have proposed to account for capillary suction in their models in order to better represent P- and/or S-wave characteristics. Shen et al. (2016) proposed an approach to invert the fluid distribution characteristics, meaning homogeneous or patchy distributions, of a 60-cm-depth sand tank from V_p, V_s, and water saturation profiles. They found that seismic measurements can be better described by contemplating different pore fluid distribution patterns, that is, homogeneous or patchy pore fluid distributions, at each particular stage of imbibition or drainage. Suzaki et al. (2017) studied S-wave velocity changes in a partially saturated surficial (6-m depth) soil embankment. These authors used a combination of empirical relationships to include suction effects into the shear modulus of the medium. Their results show that V_s measurements are affected by the degree of saturation of the medium. Romero-Ruiz et al. (2021) explored the effects of soil compaction on P-wave velocities in a first soil layer with an estimated thickness of 20 cm. They proposed a double-porosity soil physics model that includes the effects of capillary suction in the soil's frame. The abovementioned studies are largely complemented by experimental measurements performed in unsaturated particulate materials, which also evidence that V_p and V_s are affected by capillary forces for relatively small saturations (e.g., Cho & Santamarina, 2001; Dong & Lu, 2016; Fratta et al., 2005). To date, capillary suction effects on body-wave velocities have only been observed at soil probes and at small-scale experimental setups. In this sense, the importance of capillary suction effects on body-wave travel times and V_p/V_s at large offsets and more importantly, on surface-wave characteristics, remains largely unexplored.

This work aims to numerically explore the effects of capillary forces on surface-wave dispersion characteristics in unconsolidated soils. For this, we combine the HM and BG models, including capillary suction effects in the effective stress of the soil. We show that this approach is valid by comparing the results with laboratory data of S-wave velocities for different saturations. Then, saturation-depth profiles are obtained by solving Richards' (1931) equation. Combining the proposed rock physics model with the derived saturation profiles provides effective elastic moduli and, thus, V_p and V_s, which are depth- and saturation dependent. This information permits to simulate canonical seismic data sets, that is, body-wave travel times and surface-wave phase velocities, for different water table depths and soil textures. In order to evaluate the effects of capillary forces on seismic data in general and on surface-wave signatures in particular, we compare the proposed approach with an alternative model employed in the literature, which disregards capillary suction effects. We test the sensitivity of surface-wave dispersion and body-wave travel times to variations in water table depth and saturation profile. Finally, we discuss how the proposed method may assist the interpretation of surface-wave dispersion in response to variations in the saturation profile, which cannot be explained through conventional seismic approaches.

2. Methodology

2.1. Background

Let us consider an unconsolidated soil characterized by a 1D variation of the water content with depth z (Figure 1a). The soil is assumed (i) to be composed of a granular material and (ii) to present mechanical properties that depend on gravity and water saturation $S_w(z)$ (Figure 1b). We conceptualize this partially to fully saturated medium as a stack of n homogeneous and isotropic layers of thickness h_j, with $j = 1, .., n$, which are characterized by their water saturation $S_{w,j}$, effective bulk density $\rho_{b,j}$, and effective bulk K_j and shear μ_j moduli. The P- and S-wave velocities of the jth layer are thus given by

$$V_{p,j} = \sqrt{\frac{K_j + \frac{4}{3}\mu_j}{\rho_{b,j}}}, \tag{1}$$

$$V_{s,j} = \sqrt{\frac{\mu_j}{\rho_{b,j}}}, \tag{2}$$

respectively. The Poisson's ratio of the corresponding layer is (e.g., Mavko et al., 2020)

$$\nu_j = \frac{(V_{p,j}/V_{s,j})^2 - 2}{2[(V_{p,j}/V_{s,j})^2 - 1]}. \tag{3}$$

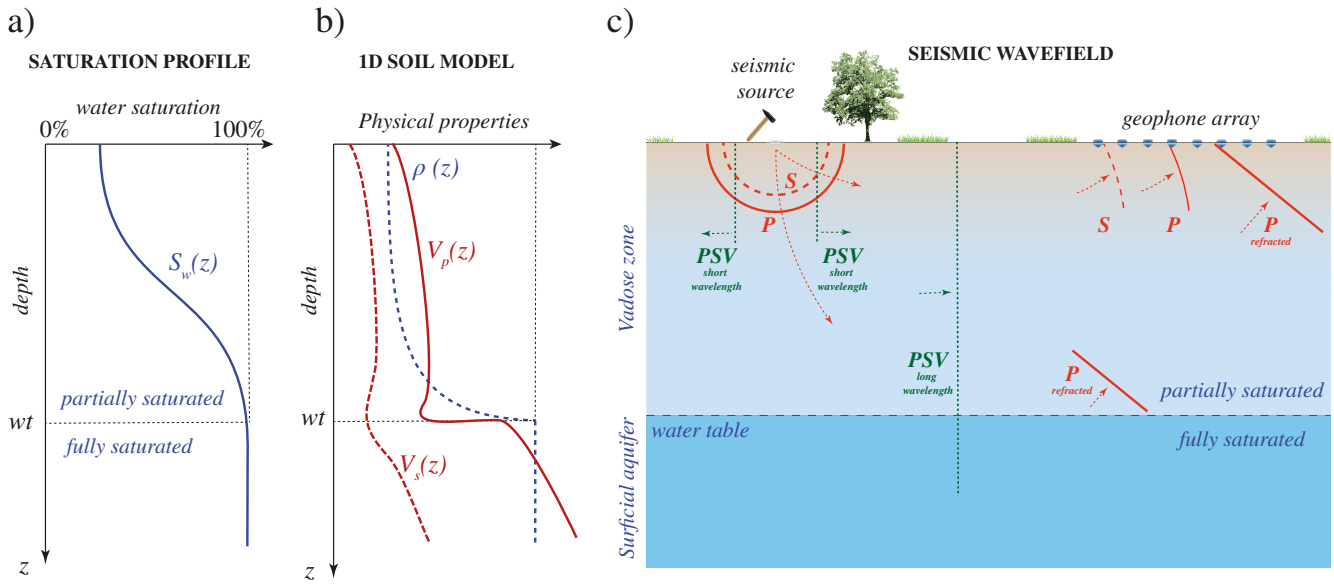

Figure 1. Schematic illustration of (a) a saturation-depth profile, which responds to Richards' (1931) equation and the van Genuchten (1980) capillary pressure saturation relationship of the soil; (b) associated density $\rho_b(z, S_w)$, P-wave velocity $V_p(z, S_w)$, and S-wave velocity $V_s(z, S_w)$ profiles; and (c) body (P and S) and surface (PSV) waves propagating in the partially saturated soil.

When the free surface of such an elastic medium is locally excited by a mechanical pulse source, such as a hammer blow, the associated perturbation propagates as elastic waves (Figure 1c). The most common paradigm in seismic applications is to consider the propagation of (a) body waves, that is, P and S waves with particle displacements describing spherical wavefronts, and (b) surface waves, namely Rayleigh and Love waves, characterized by cylindrical wavefronts.

On the one hand, classic body-wave interpretation mainly consists in analyzing travel times versus offset curves observed along a receiver array. These arrivals correspond to displacements due to direct waves at near offsets and to refracted waves (conical wavefronts) further along the line (Figure 1c). Their corresponding travel times can be easily computed from the stack of layers described above in the framework of ray theory (e.g., Herrmann, 2013; Shearer, 2019). This approach has been previously applied to the case of unconsolidated sands (Bachrach et al., 1998, 2000; Vriend et al., 2007) and more recently to glass bead models (Bergamo et al., 2014; Bodet et al., 2014; Pasquet, Bodet, et al., 2016). In this context, better travel time estimations are obtained as one considers a larger number of layers to discretize the probed medium (e.g., Shearer, 2019). As further detailed in the following sections, we employ a very large number of layers (as compared with the depth of the probed media) to adequately approximate the continuous variations of the model properties with depth. To reduce the associated high computational costs, future parametric studies of this kind will require optimization, such as the use of interpolation functions or nonlinear staircase models (e.g., Bergamo & Socco, 2016).

On the other hand, surface waves arise from constructive interference between body waves in the presence of a free surface, which acts as a wave guide. Surface waves only propagate along this free surface and their amplitudes decay exponentially with depth. As such, they mainly sense the properties of a limited surficial region whose thickness is related to the corresponding wavelength (Figure 1c). This implies that, in media presenting variations in their properties with depth, the phase velocities of surface waves exhibit a pronounced frequency-dependent behavior or dispersion. In this work, we focus on Rayleigh waves, resulting from constructive interference between P and vertically polarized S waves (PSV), which tend to be dominant in most experimental studies when using vertical-component geophones. To simulate Rayleigh-wave dispersion curves, we use the classical Thomson-Haskell matrix propagator technique (Haskell, 1953; Herrmann, 2013; Thomson, 1950) in a stack of $n-1$ layers over a half-space (layer n). This approach was previously employed to study unconsolidated granular materials (e.g., Bergamo et al., 2014; Bodet et al., 2014). We analyze the fundamental PSV propagation mode, as it is empirically known to be representative of the medium structure and frequently more energetic than the other wave modes (e.g., Foti et al., 2018; Socco & Strobbia, 2004), which, in turn, allows for a reliable

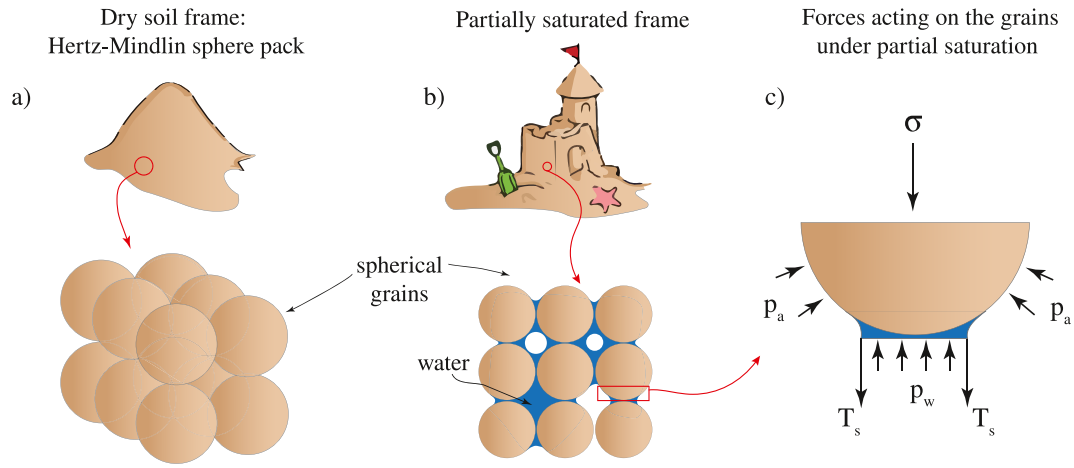

Figure 2. Schematic illustration of (a) a dry soil, which is conceptualized as an arrangement of spherical particles, (b) the stiffening effect associated with the partially saturated state, and (c) the stresses acting on the grains, which determine the effective stress P_e. We indicate the direction of the stress components associated with the overburden stress σ, the air and water pressures p_a and p_w, respectively, and the capillary tension T_s.

identification in real data. It is important to remark that, even though not studied here, higher order modes also contain important information (e.g., Gabriels et al., 1987) and should be included in inversion or interpretation processes when available.

2.2. Elastic Properties of a Partially Saturated Soil

2.2.1. Elastic Properties of the Soil's Frame

In order to model the behavior of surface waves in partially saturated soils, we need to estimate the effective elastic properties of the soil's frame, that is, the so-called *drained moduli* of the porous medium K_m and μ_m (Berryman, 1999). For this, we use the Hertz-Mindlin (HM) model, which has proven its pertinence in a wide variety of related scenarios (e.g., Bachrach et al., 1998; Pasquet, Holbrook, et al., 2016; Shen et al., 2016). This model conceptualizes the soil's frame as a pack of spherical particles (Figure 2a) whose effective bulk and shear moduli are given by (e.g., Mavko et al., 2020)

$$K_m(z,\ S_w) = \left[\frac{N^2(1-\phi)^2\mu_s^2}{18\pi^2(1-\nu_s)^2}P_e(z,S_w)\right]^{\frac{1}{3}}, \tag{4}$$

$$\mu_m(z,S_w) = \frac{2+3f-(1+3f)\nu_s}{5(2-\nu_s)}\left[\frac{3N^2(1-\phi)^2\mu_s^2}{2\pi^2(1-\nu_s)^2}P_e(z,S_w)\right]^{\frac{1}{3}}, \tag{5}$$

where ϕ is the porosity, $P_e(z, S_w)$ is the saturation- and depth-dependent effective stress, N is the average number of contacts per particle in the sphere pack, and f is the fraction of nonslipping particles. Based on previous work (Bachrach & Avseth, 2008; Dvorkin et al., 1999; García & Medina, 2006; Murphy, 1982), we take N and f as constant parameters. Note that these parameters may indeed present stress-dependent characteristics, which are, however, beyond the scope of this study. μ_s and ν_s denote the effective shear modulus and Poisson's ratio of the solid grains, respectively, with

$$\nu_s = \frac{3K_s - 2\mu_s}{2(3K_s+\mu_s)}, \tag{6}$$

where K_s denotes the effective bulk modulus of the corresponding grains. If the soil is composed of several constituents, the elastic moduli of the grains can be computed from the individual constituent properties using Hill's averaging formula (e.g., Dvorkin et al., 1999; Hill, 1952)

$$K_s = \frac{1}{2}\left[\sum_{i=1}^{m}\gamma_i K_{s,i} + \left(\sum_{i=1}^{m}\frac{\gamma_i}{K_{s,i}}\right)^{-1}\right], \quad \mu_s = \frac{1}{2}\left[\sum_{i=1}^{m}\gamma_i \mu_{s,i} + \left(\sum_{i=1}^{m}\frac{\gamma_i}{\mu_{s,i}}\right)^{-1}\right], \tag{7}$$

where m is the number of constituents, γ_i is the corresponding volumetric fraction, and $K_{s,i}$ and $\mu_{s,i}$ are the bulk and shear moduli of the ith constituent, respectively. Correspondingly, the effective density of the solid grains is given by $\rho_s = \sum_{i=1}^{m}\gamma_i\rho_{s,i}$.

Equations 4 and 5 allow us to estimate the elastic moduli of the soil's frame. For this, we first need to analyze the effects of partial saturation on the effective stress $P_e(z, S_w)$.

2.2.2. Capillary Effects on Effective Stress

The mechanical properties of unconsolidated soils do not behave as those of consolidated rocks with varying saturation. When studying consolidated rocks, the frame moduli K_m and μ_m depend on the solid grain properties K_s and μ_s, the porosity ϕ, and on the degree of consolidation (e.g., Pride, 2005). A classic, and rather simple, procedure to estimate the moduli K_m and μ_m of a consolidated rock sample is to measure its dry (air-saturated) response (Mavko et al., 2020). Notably, the frame moduli K_m and μ_m of a consolidated rock are independent of the degree of saturation, as they are essentially matrix properties. However, evidence shows that unconsolidated soils do not behave as consolidated rocks in this regard, as soil frame properties are highly sensitive to the saturation S_w. An illustrative example of this characteristic is the stability of sandcastles (Figure 2b). When water is added to the unconsolidated soil, air and water pore fluid pressures, p_a and p_w, respectively, oppose the lithostatic overburden stress σ (Figure 2c). On top of that, capillary tension T_s pulls soil particles together (Figure 2c). As a result of this effect, usually referred to as capillary suction, the shear strength of unconsolidated porous media may increase (e.g., Hornbaker et al., 1997; Z.; Lu & Sabatier, 2009).

Bishop and Blight (1963) proposed an approach to empirically account for the above-described effects in Terzaghi's (1923) classic effective stress definition, which yields (e.g., N. Lu et al., 2010; Romero-Ruiz et al., 2021; Shen et al., 2015)

$$\begin{aligned} P_e(S_w) &= \sigma(S_w) - p_a[1-\chi(S_w)] - p_w\chi(S_w), \\ &= \sigma(S_w) - p_a + \chi(S_w)p_c(S_w), \\ &= \sigma(S_w) - p_a + \sigma_s(S_w), \end{aligned} \tag{8}$$

where $\sigma = \rho_b(S_w)gz$ is the overburden stress and $p_\zeta = \rho_j gz$, with $\zeta = a, w$, are the air and water pore fluid pressures, respectively, with ρ_j being the fluid density, and $g = 9.806\ \mathrm{ms}^{-2}$ the Earth's gravitational acceleration. Note that $p_c(S_w) = p_a - p_w$ denotes the capillary pressure, which is commonly related to the degree of saturation through suitable constitutive models (e.g., van Genuchten, 1980). The term $\sigma_s = \chi(S_w)p_c(S_w)$ is usually referred to as capillary suction stress. The effective stress parameter $0 < \chi(S_w) < 1$ is a function of the local saturation of the soil that allows to integrate capillary effects into macroscopic behavior. Many authors argue that it can be approximated by the effective saturation of the medium $\chi = S_{we} = (S_w - S_{wr})/(1 - S_{wr})$, with S_{wr} denoting the residual water saturation (N. Lu & Likos, 2006; Nuth & Laloui, 2008; Shen et al., 2016). This implies that, for fully water-saturated soil, we have $\chi = 1$ and thus, Equation 8 becomes equivalent to Terzaghi's classic effective stress relation for fully saturated media, that is, $P_e = \sigma - p_w$. Note that the Biot-Willis coefficient is assumed to be close to unity, as is indeed a common practice when dealing with unconsolidated materials (e.g., Bachrach & Avseth, 2008).

When including Equation 8 in Equations 4 and 5, we retrieve the effective moduli of the soil's frame K_m and μ_m, which, as described above, depend on the water content. To obtain the overall bulk K and shear μ moduli of the partially saturated medium, involved in Equations 1 and 2, we use Gassmann's (1951) equations.

2.2.3. Biot-Gassmann Equations

The Biot-Gassmann low-frequency relationships are classically used to account for the effects of a saturating fluid on the elastic moduli of porous materials. They are given by Gassmann (1951)

$$K(z,S_w)=K_m(z,S_w)+\frac{\left(1-\frac{K_m(z,S_w)}{K_s}\right)^2}{\frac{\phi}{K_f(S_w)}+\frac{1-\phi}{K_s}-\frac{K_m(z,S_w)}{K_s^2}}, \tag{9}$$

$$\mu(z,S_w)=\mu_m(z,S_w), \tag{10}$$

where K_f is the fluid bulk modulus and K_m and μ_m are the drained moduli of the porous medium. Equations 9 and 10 assume that all pores are connected and that pore fluid pressures are able to equilibrate throughout the porous medium. Given that Gassmann's equations were derived for monosaturated porous media, we use, from now on, effective moduli to account for the effects of partial saturation on K_m, μ_m, and K_f. We thus follow the common assumption that the functional form of Equations 9 and 10 is maintained.

On the one hand, we use effective values for $K_m(z,S_w)$ and $\mu_m(z,S_w)$, derived from Equations 4 and 5, respectively. This allows to account for the effects of overburden and capillary suction on the frame elastic moduli of unconsolidated soils. On the other hand, we use an effective fluid bulk modulus $K_f(S_w)$. For this, we consider that, for sufficiently low frequencies, internal pore fluid pressure gradients generated by a passing seismic wave have time to equilibrate during a half-cycle and thus, the elastic properties of the pore fluid components can be approximated by (e.g., Bachrach et al., 1998; Shen et al., 2016)

$$K_f(S_w)=\left[\frac{S_w}{K_w}+\frac{1-S_w}{K_a}\right]^{-1}, \tag{11}$$

with K_w and K_a denoting the bulk moduli of water and air, respectively. The combination of Equations 11 and 9 results in the so-called Biot-Gassmann-Wood approximation for partially saturated porous media (e.g., Mavko et al., 2020). Similarly, the bulk density is given by

$$\rho_b(S_w)=(1-\phi)\rho_s+\phi[S_w\rho_w+(1-S_w)\rho_a]. \tag{12}$$

where ρ_a and ρ_s denote the density of air and of the solid grains, respectively.

In order to reconcile Equations 9–12 with Equations 1 and 2, expressing the variation of V_p and V_s with depth, we need the corresponding saturation profile $S_w(z)$, which, as shown below, is associated with the hydraulic properties of the soil.

2.3. Saturation Profile

Once again, let us assume that the soil is a homogeneous and isotropic 1D porous medium, for which water flow obeys Richards' equation (Richards, 1931)

$$\frac{\partial}{\partial z}\left(\mathcal{K}(h)\frac{\partial}{\partial z}(h+z)\right)-\phi\frac{\partial S_w(h)}{\partial t}=0, \tag{13}$$

where $\mathcal{K}$ is the hydraulic conductivity and $h=-p_c/\rho_w g$ is the hydraulic pressure head. Both $\mathcal{K}$ and S_w are functions of the pressure head h. Equation 13 is a classical model in hydrology that assumes that the non-wetting phase (air) is infinitely mobile and, thus, p_a variations in the subsurface are negligible. Consequently, the hydraulic pressure head can be approximated by $h\simeq p_w/\rho_w g$. In Equation 13, Darcy's flow is deemed valid for the wetting phase for the entire saturation range. This assumption implies that a continuous, interconnected, and potentially very tortuous wetting fluid phase exists throughout the porous medium. This state is usually referred to as capillary or funicular regime. For sufficiently small saturations, the soil approaches the residual saturation state $S_{w,r}$. Beyond this point, that is, for $S_w<S_{wr}$, the medium is in the so-called pendular regime, where isolated water droplets prevail surrounding grains and thus, Equation 13 is no longer valid. Note that reaching the pendular regime requires evaporation processes, which are beyond the scope of this work.

In order to solve Equation 13, initial and boundary conditions as well as suitable constitutive relationships for $S_w(h)$ and $\mathcal{K}(h)$ must be defined. In particular, we employ van Genuchten's (1980) constitutive model to relate S_{we} and h, which responds to

$$S_{we}(h) = \begin{cases} [1 + (\alpha_{vg} h)^{n_{vg}}]^{-m_{vg}}, & \text{for} \quad h < 0, \\ 1, & \text{for} \quad h \geq 0, \end{cases} \tag{14}$$

where α_{vg} [m^{-1}] denotes the inverse of the entry pressure, a value related to the air pressure needed to displace water from the larger pore sizes, and n_{vg} [-] and $m_{vg} = 1 - 1/n_{vg}$ are parameters related to the pore size distribution (Carsel & Parrish, 1988; Guarracino, 2007). Given that $h = -p_c/\rho_w g$, we can use Equation 14 in Equation 8 to relate S_w to the capillary suction stress σ_s.

For simplicity, let us consider that the vadose zone is in equilibrium, that is, that the water is immobile. In this context, S_w does not vary with time and thus, Equation 13 reduces to

$$\frac{\partial}{\partial z}\left(\mathcal{K}(h)\frac{\partial}{\partial z}(h + z)\right) = 0. \tag{15}$$

In addition, Darcy's flow is null, that is, $\mathcal{K}(h)\frac{\partial}{\partial z}(h + z) = 0$. Consequently, the result of Equation 15 is given by $h + z = c$ with c being an integration constant. If we take $z = 0$ at the Earth's surface, $h = 0$ at the water table, and employ Equation 14, we get (e.g., Zyserman et al., 2017)

$$S_{we}(z) = \begin{cases} \left\{1 + [\alpha_{vg}(\text{wt} - z)]^{n_{vg}}\right\}^{-m_{vg}}, & \text{for} \quad z < \text{wt}, \\ 1, & \text{for} \quad z \geq \text{wt}, \end{cases} \tag{16}$$

where wt denotes the depth of the water table. An illustration of a typical saturation profile obtained using this procedure is given in Figure 1a.

3. Results

In this section, we numerically analyze the effects of capillary suction on surface waves in unconsolidated soils. First, we describe the effects of capillary suction on P- and S-wave velocities as functions of saturation. Then, we analyze the capillary effects on Poisson's ratios, body-wave travel times, and surface-wave dispersion in a partially saturated soil for different saturation-depth characteristics. Finally, we study the behavior and the dispersion characteristics of surface waves in response to variations in the saturation profile.

3.1. Capillary Effects on V_p and V_s

In the following, we briefly illustrate how capillary suction influences V_p and V_s curves for different saturations and soil textures comparing the proposed model with laboratory measurements. In order to discern capillary suction effects on body-wave velocities from those related to changes in bulk density $\rho_b(S_w)$ and/or effective fluid bulk modulus $K_f(S_w)$, which are also affected by saturation, we compare the proposed approach with an alternative model, present in the literature, which assumes that the effective stress depends solely on the net overburden stress $P_e = \sigma$ (e.g., Bachrach et al., 1998; Pasquet, Holbrook, et al., 2016).

Figure 3 shows a comparison of the proposed model with experimental data retrieved by Dong and Lu (2016), who studied S-wave velocities in different soil samples for varying saturations. We focus here on two soils with different characteristics: *Missouri clay* ($\phi = 0.49$) and *Esperance sand* ($\phi = 0.419$). We consider measurements during drying for which the saturation lies in the funicular (capillary) regime, that is, we disregard measurements for which saturations are below $S_{w,r}$, as they cannot be achieved by fluid flow techniques. K_s and μ_s are derived by assuming the soils are composed of a mixture of kaolinite (Ka) and quartz (Qz) grains. For the Missouri clay, we consider the proportions $\gamma_{Ka} = 0.9$ and $\gamma_{Qz} = 0.1$ (Equation 7). Conversely, for the Esperance sand, we consider $\gamma_{Ka} = 0.3$ and $\gamma_{Qz} = 0.7$. Given that, in all cases, Dong and Lu's (2016) measurements were performed in soil samples of approximately 20-mm thickness, we assume that the overburden is $\sigma = \rho_b(S_w)gz^*$, with $z^* = 10$ mm

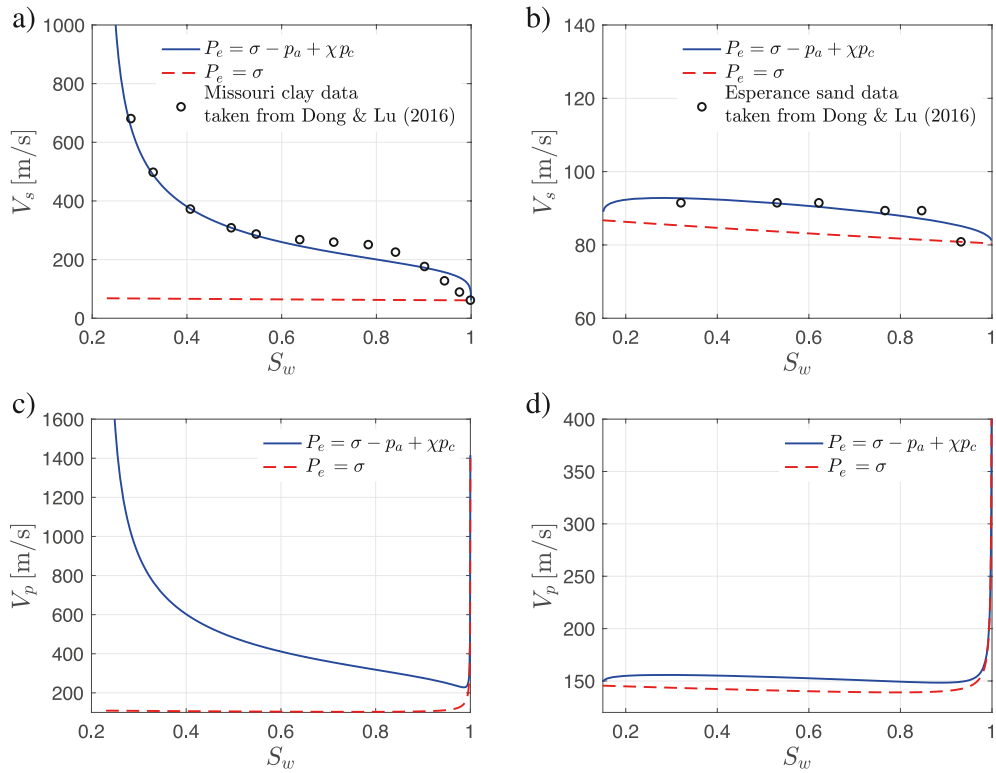

Figure 3. (a and b) S- and (c and d) P-wave velocities as functions of saturation for Missouri clay (left column) and Esperance sand (right column). S-wave velocity measurements taken by Dong and Lu (2016) in the funicular (capillary) regime are represented using circles. We illustrate the fitted behavior of the proposed model (blue solid lines), which includes capillary suction effects, and the behavior of the associated net overburden stress model (red-dashed lines), which disregards capillary suction effects.

being an effective depth. The properties of the van Genuchten (1980) model (Equation 14) that best fit the data with respect to the L_2 norm are summarized in Table 1. The properties of the components as well as those of the pore fluids (water and air) are summarized in Table 2.

Figure 3 shows V_s and V_p variations with saturation for the proposed model (blue solid lines), the associated net overburden stress model (red-dashed lines), and the laboratory measurements of S-wave velocities of Dong and Lu (2016) (circles). In Figure 3a, we observe that the model that accounts for capillary suction effects is able to correctly represent the V_s increase with decreasing saturations S_w in the Missouri clay, which is associated with the stiffening effect of capillary forces. The associated relative error with respect to the L_2 norm is $e = 0.083$. However, the corresponding net overburden stress model cannot correctly describe the behavior of V_s for this soil texture, showing a relative error of $e = 0.82$. This evidences that bulk density variations alone cannot explain the S-wave velocity change with S_w, thus making the incorporation of capillary suction effects a key aspect for modeling the seismic response of the soil. In the case of the Esperance sand (Figure 3b), once again the model comprising capillary effects is better suited for representing the V_s data. However, in this case, the differences between the proposed approach and the net overburden stress approach are smaller than those observed for the Missouri clay, as they present relative errors of $e = 0.023$ and $e = 0.07$, respectively. Figures 3c and 3d show V_p variations with S_w for the Missouri clay and the Esperance sand, respectively. By comparing the proposed approach and the net overburden stress model, we observe that capillarity is a preeminent cause for P-wave velocity increases at relatively low saturations in the Missouri clay. However, the corresponding difference is relatively small for the Esperance sand.

Table 1
Mechanic and Hydraulic Properties of Soils Employed in the Numerical Experiments

Soil Type	ϕ	S_{wr}	n_{vg}	α_{vg} [cm^{-1}]	N	f
Esperance sand	0.419	0.15	2.36	0.67	6	0.1
Missouri clay	0.49	0.23	1.28	0.0013	8	0.3
Sandy clay	0.38	0.26	1.23	0.027	8	0.3

Note. Esperance sand and Missouri clay properties, aside from the porosity (Dong & Lu, 2016), are fitted using the model proposed in Section 2.2. Water retention parameters for Sandy Clay are taken from Carsel and Parrish (1988).

Table 2
Properties of Mineral Components and Pore Fluids Used in This Work, Taken From Mavko et al. (2020)

Minerals	ρ_s [kg/m^3]	K_s [GPa]	μ_s [GPa]
Quartz (Qz)	2,600	45	36
Kaolinite (Ka)	1,580	1.5	1.4
Gulf clay (Gc)	2,550	7	25
Fluids	$\rho_{w,a}$ [kg/m^3]	$K_{w,a}$ [GPa]	
Water	1,000	2.3	
Air	1	1×10^{-4}	

Dong and Lu's (2016) observations, together with other studies in the literature (e.g., Cho & Santamarina, 2001; Fratta et al., 2005), evidence that capillary suction effects on V_p and V_s decrease as soil textures become coarser. In the following, we thus concentrate the analysis of capillary effects on surface-wave dispersion using properties of medium-to fine-grained soils, for which capillary suction effects are expected to be predominant. However, it is important to remark here that the relative contribution of capillary suction to the effective stress (Equation 8) is maximal at low overburden stresses. Conversely, the effects of capillary suction on the effective stress and thus, on the seismic velocities, are expected to decrease with increasing depth irrespective of the soil texture.

3.2. Capillary Effects on Surface-Wave Dispersion

Let us now analyze the effects of capillary suction on surface-wave dispersion curves. For this, we consider a numerical model consisting of a 192-m-long, 2-m-spaced, linear geophone array, emulating a typical field setup. As previously mentioned, in all numerical examples and for both travel time and velocity dispersion computations, we use a very fine discretization of the 1D models, consisting of 12,000 layers to represent the saturation profile in the vadose zone ($z < 25$ m). We consider that the vadose zone is composed of a Sandy clay soil (Table 1), whose constituents are Gulf clays ($\gamma_{GC} = 0.43$) and Quartz ($\gamma_{Qz} = 0.57$) grains (Table 2). The saturation profile is obtained by solving Equation 16 assuming that the water table is located at 25-m depth (Figure 4a). Recall that the soil's bulk density $\rho_b(z)$, given by Equation 12, changes with the saturation (Figure 4b). Again, we consider the models analyzed in Figure 3: (i) overburden stress $P_e = \sigma$ only (red-dashed lines) and (ii) the effective stress proposed in this study accounting for capillary suction effects $P_e = \sigma - p_a + \chi p_c$ (blue solid lines).

Given that surface waves arise from the constructive interference of body waves, let us first analyze the effects of capillary suction on P- and S-wave profiles and Poisson's ratios in depth. We note that both $V_p(z)$ and $V_s(z)$ obtained from the proposed model present larger values than the net overburden model for $z < 10$ m (Figures 4c and 4d). This is expected as capillary suction forces tend to increase the velocities of body waves in soils for relatively low saturations (Figure 3), which, for the considered saturation profile, are located near the surface. We observe that, while the two models present different characteristics for the $V_p(z)$ and $V_s(z)$ curves, both of them predict a small inflection, with reduced local velocities, just above the water table, which results from the effect of the increasing density on velocities right before full saturation. Furthermore, for both models, V_p naturally increases as soon as the water table is reached (Figure 4c), mainly as a consequence of a strong increase of the effective fluid bulk modulus $K_f(S_w)$. On the other hand, V_s naturally decreases for both models as soon as the water table is reached (Figure 4d), which is a consequence of an increase in the bulk density. It is also interesting to note that, even though $V_p(z)$ and $V_s(z)$ for these models present notable differences, the corresponding Poisson's ratio profiles are remarkably similar (Figure 4e). This characteristic implies that Poisson's ratios and thus, the associated V_p/V_s ratios are largely insensitive to pore-scale rock physics. Since Poisson's ratios remain almost constant in the unsaturated part, this attribute only allows for discerning fully saturated regions from partially saturated regions of the soil.

As previously mentioned, P and S waves are not expected to be particularly sensitive to capillary suction effects in coarse-grained soils. However, even in medium-to fine-grained soils, such as sandy clay, it is still not clear how strong these effects are on body-wave travel times and whether they can be discernible in seismic recordings. By analyzing synthetic P- and S-wave travel times computed from the velocity structures shown in Figures 4a–4d, we note that the two P_e models result in remarkably similar estimates (Figures 4f and 4g). P-wave travel times corresponding to the refraction from the water table (Figure 4f) naturally show similar slopes (apparent velocities). Yet, the intercept times are different, as the unsaturated zones of the two models do not present the same gradients (Figure 4f). This difference can actually also be anticipated from slopes of travel time curves at short offsets. For the S-wave travel times (Figure 4g), the two models show a slight nonlinear increase with offset. Because of the low-velocity zone, S-wave travel times neither inform about the water table depth nor about velocities in

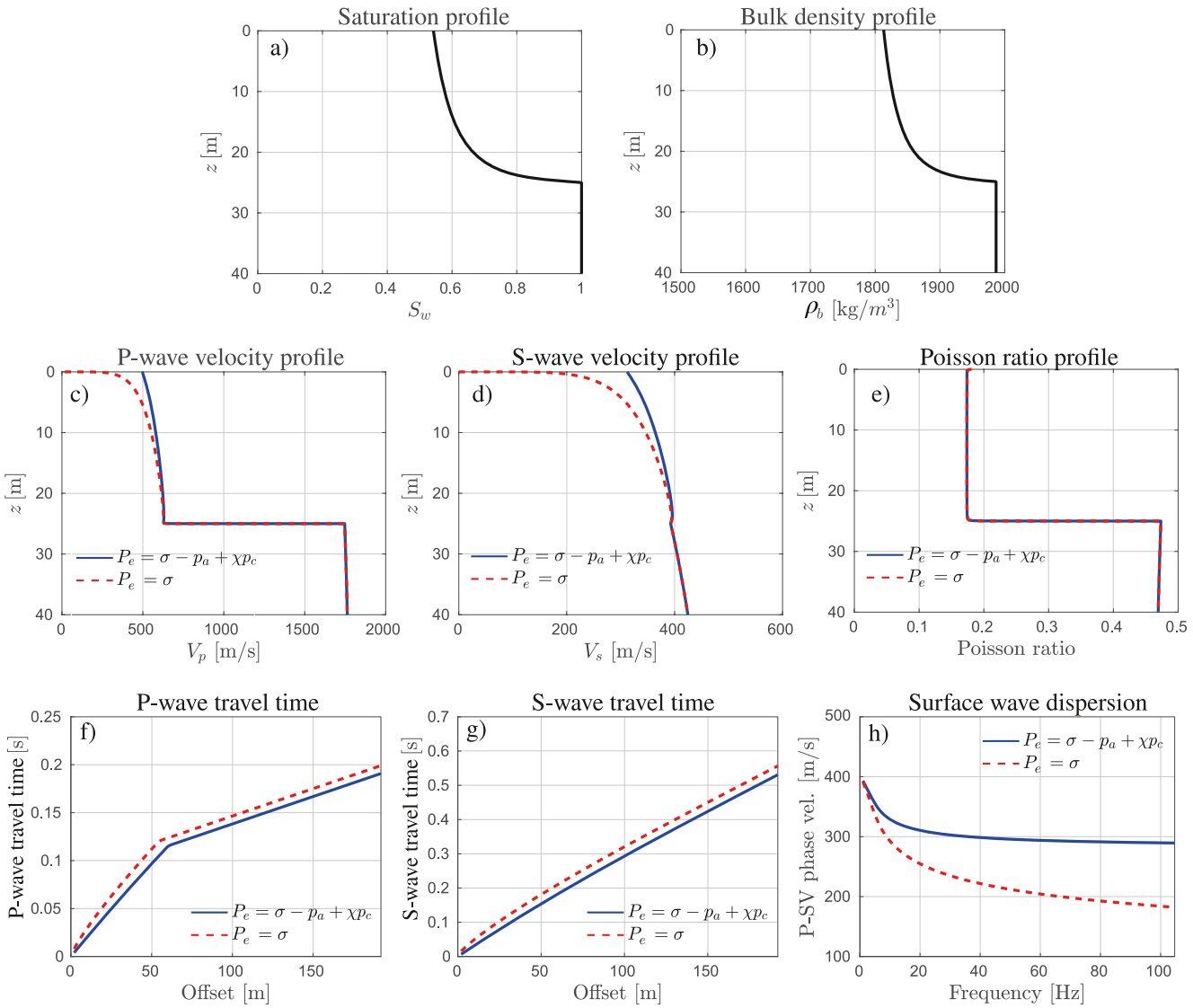

Figure 4. Sandy clay-type soil model with the water table at $z = 25$ m. (a) Water saturation; (b) bulk density; (c) P-wave velocity; (c) S-wave velocity; and (e) Poisson's ratio. The bottom row illustrates the corresponding (d) P- and (e) S-wave travel times and the (f) surface-wave phase velocity as a function of frequency. Red-dashed lines represent net overburden stress; blue solid lines represent proposed model accounting for suction effects.

the saturated layers. Note that, in a field case scenario, where measuring errors and noise are present, the two P_e models could be equally employed to interpret the travel times of P and S waves.

Conversely, the synthetic surface-wave dispersion curves show remarkably different characteristics for the two P_e models (Figure 4h). The dispersion curves are consistent with a positive rigidity gradient, that is, they show increasing velocities for decreasing frequencies. The important feature here is the difference between these two models with increasing frequency, which is related to the differences in V_s at shallow depth ($z < 10$m). These observations imply that, while different physical models of the same soil type may result in similar P- and S-wave travel times and Poisson's ratio profiles, the phase velocity dispersion of surface waves is strongly affected by capillary forces acting in the partially saturated zone.

3.3. Effects of the Saturation Profile on Surface-Wave Dispersion

Models employed to interpret surface-wave dispersion characteristics should be capable of accounting for the observed variations associated with changes in the saturation profile (Bodet, 2019; Dangeard et al., 2018; Z.;

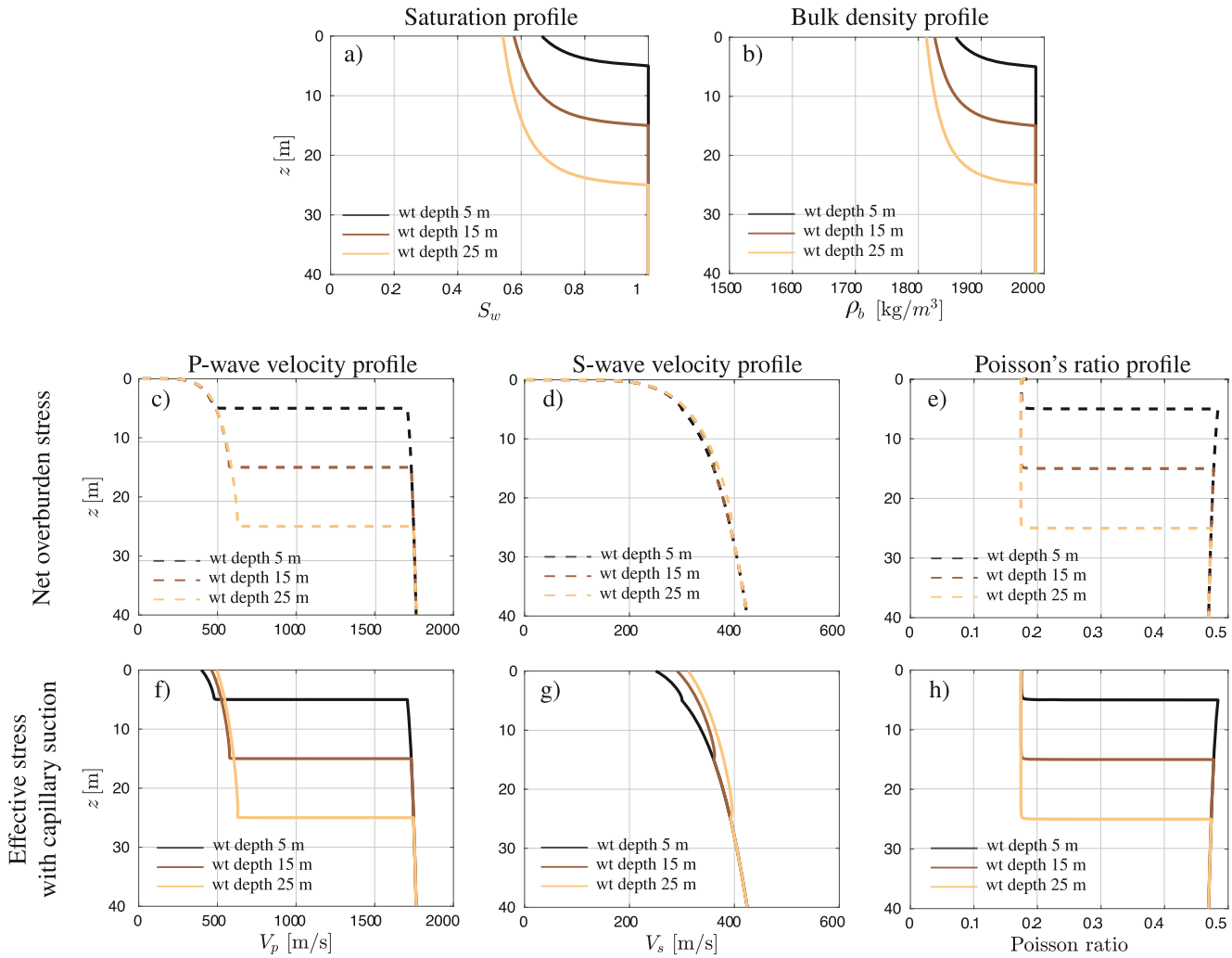

Figure 5. Sandy clay-type soil model for three different water table depths: 5 m (black lines), 15 m (brown lines), and 25 m (light brown lines). (a) Water saturation; (b) bulk density; (c and f) P-wave velocity; (d and g) S-wave velocity; and (e and h) Poisson's ratio. The second and third rows illustrate the behavior considering net overburden stress $P_e = \sigma$ only (dashed lines) and the proposed approach $P_e = \sigma - p_a + \chi p_c$ (solid lines), respectively.

Lu, 2014; Pasquet, Bodet, et al., 2016; West & Menke, 2000), as, failing to do so, results in an erroneous characterization of the medium. In the following, we illustrate that capillary suction must be accounted for in the underlying effective stress to allow for a correct interpretation of the observed surface-wave dispersion characteristics. For this purpose, we again consider a sandy clay-type soil model (Tables 1 and 2) and the same source-geophone array as in the previous section. We explore three different saturation profiles, obtained by assuming that the water table depth is static and located at depths of 5, 15, and 25 m (Figure 5a). Note that the corresponding saturations, which are obtained by solving Equation 16 using the properties given in Table 1, greatly differ. With regard to the effective soil stress, we again consider the two models analyzed previously, that is: (a) overburden stress $P_e = \sigma$ only and (b) effective stress accounting for capillary suction effects $P_e = \sigma - p_a + \chi p_c$.

The $V_p(z)$ profiles resulting from the model accounting for capillary suction effects present some small differences for $z < 5$ m when compared to the net overburden stress model when the water table and the respective saturation profile change (Figures 5c and 5f). Conversely, $V_s(z)$ profiles obtained by considering suction effects present more significant discrepancies with regard to the net overburden model (Figures 5d and 5g). The interesting feature here is the slight increase of V_s for $z < 20$ m when saturation decreases in the vadose zone due to the greater depth of the water table. As previously observed in Figure 4, Poisson's ratios for the two models are remarkably similar when changing the water table depth (Figures 5e and 5h). This result provides further evidence

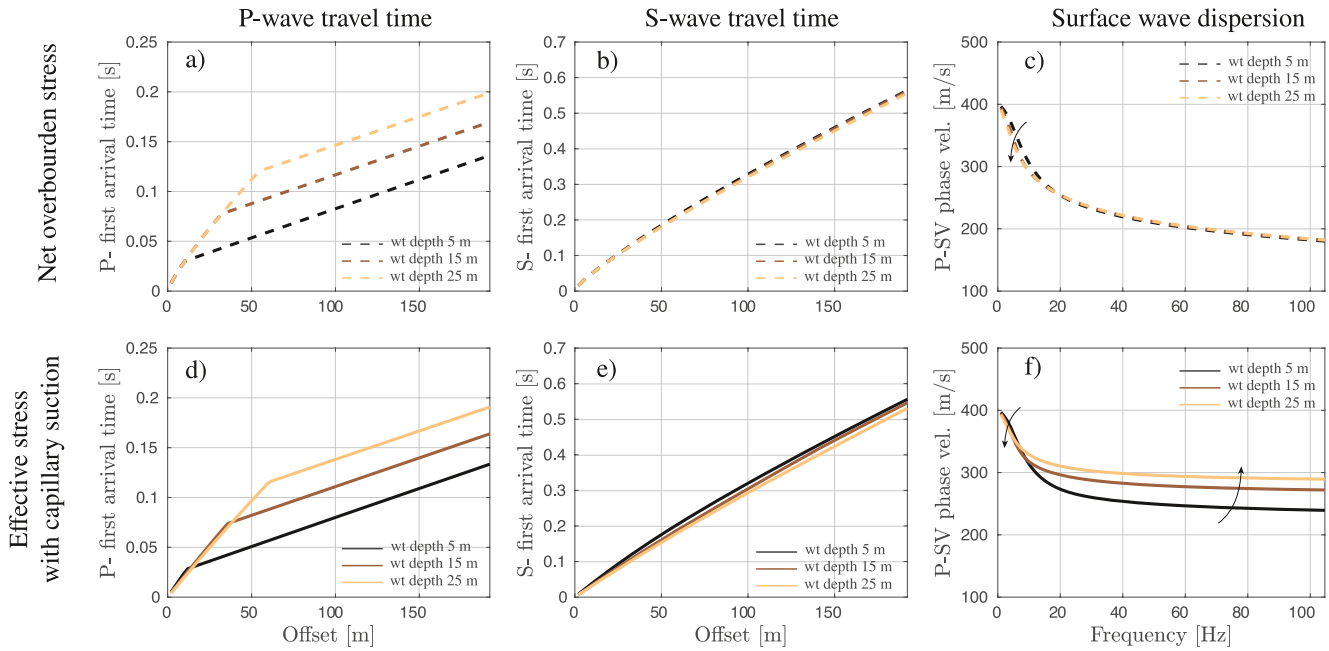

Figure 6. (a, d, g) P-wave and (b, e, h) S-wave travel times, and (c, f, i) the surface-wave phase velocity as a function of frequency for a sandy clay-type soil. We consider three different water table depths: 5 m (black lines), 15 m (brown lines), and 25 m (light brown lines). The first and second rows illustrate the behavior considering net overburden stresses $P_e = \sigma$ only (dashed lines) and of the proposed model $P_e = \sigma - p_a + \chi p_c$ (solid lines), respectively.

that Poisson's ratios and, thus, V_p/V_s estimates permit to discern the location of the water table, irrespective of the employed rock physics model, while they do not allow to discern the characteristics of the saturation profile.

When analyzing the P-wave (Figures 6a and 6d) and S-wave (Figures 6b and 6e) travel times, it transpires that the two models result in similar data, which exhibit comparable features. The variation of these curves is mainly driven by changes in the water table depth, which is more evident in P-wave data. The related changes in the saturation profiles of course do have effects at short offsets and on the S-wave travel times, but again, as explained in the previous section, variations in observed travel time data are small compared to absolute values, indicating once again that capillary suction effects do not seem to have a large effect on body-wave travel times even in medium-to fine-grained soils where capillary suction effects are expected to be important.

Interestingly, when considering net overburden stresses as the sole cause of the effective pressure (Figure 6c), surface-wave dispersion curves show a slight decrease in velocities with increasing water table depth in the 0–20 Hz frequency range with relative velocity changes of up to −6.88%. A similar behavior was observed by West and Menke (2000) at frequencies below 40 Hz at a sandy beach undergoing variations in the water table depth. Aside from this, dispersion curves do not appear to be significantly affected by the water table depth or the associated partially saturated zone. However, the proposed model, involving suction effects, results in surface-wave dispersion curves, which show a strong dependency on the water table depth and on the overlaying partially saturated zone (Figure 6f). The downward shift observed previously in Figure 6c is also present in Figure 6f, yet it is shifted toward a lower frequency. We also observe that dispersion curves show an upward shift in the 10–100 Hz frequency range with a maximum relative velocity change of 20.75%, which is indicated by the corresponding arrow in Figure 6f. This trend is associated with increasing capillary suction effects in the vadose zone when the water table descends. A similar behavior was observed, for instance, by Z. Lu (2014) during extended dry periods in a sandy soil for frequencies ranging from 40 to 400 Hz.

4. Discussion

Field measurements indicate that surface-wave dispersion in unconsolidated granular media is sensitive to changes in the saturation profile (e.g., Bodet, 2019; Dangeard et al., 2018; Z.; Lu, 2014; Pasquet, Bodet, et al., 2016; West & Menke, 2000). However, the interpretation of such changes is not an easy task, mainly because most

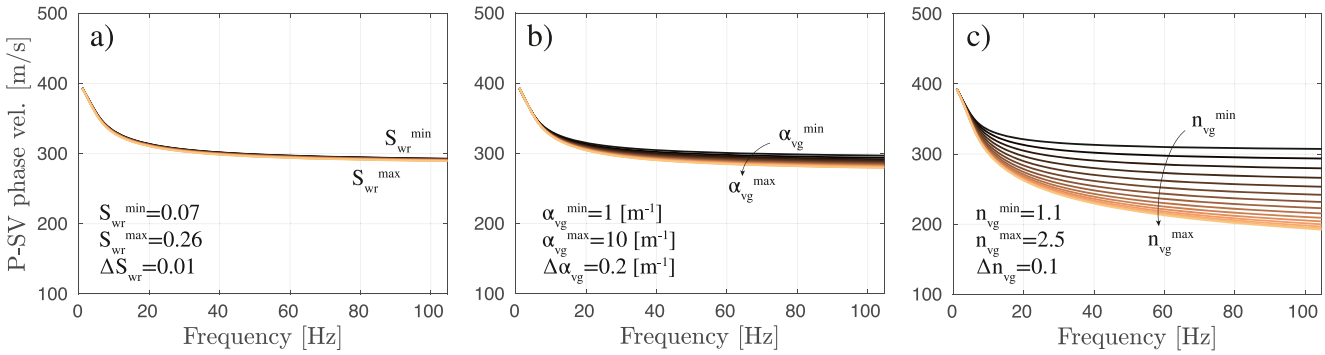

Figure 7. Surface-wave phase velocity as a function of frequency for different values of the van Genuchten (1980) parameters S_{wr}, α_{vg}, and n_{vg}. We vary (a) S_{wr}, (b) α_{vg}, and (c) n_{vg} parameters between maximum and minimum characteristic values provided by Carsel and Parrish (1988) for typical soil textures.

rock physics models are developed to fit body-wave travel times, which in turn, appear to be rather insensitive to changes in the saturation profile in the vadose zone. Our results show that this apparent difference in sensitivity can be explained by the fundamental physical characteristics of body and surface waves.

Body waves are influenced by material property variations along their path, which in turn, are largely dominated by the velocity gradients with depth. As such, they sense the medium's properties between the source and a given receiver up to a maximum penetration depth, which, in the given context, essentially depends on the offset. The longer the offset, the greater the depth of investigation. Only strong contrasts in the material properties generate discernible changes in the slopes of the travel time versus offset curves. Correspondingly, P- and S-wave data are mainly sensitive to water table depth variations. This also explains why V_p/V_s and Poisson's ratio attributes are robust to detect water table depth (e.g., Konstantaki et al., 2013; Pasquet, Bodet, Dhemaied, et al., 2015; Pasquet, Bodet, Longuevergne, et al., 2015) but generally do not allow to quantify changes in saturation in the overlying vadose zone (e.g., Blazevic et al., 2020; Dangeard et al., 2018).

The observed sensitivity of surface-wave phase velocity dispersion to changes in the saturation profile can be explained by the way Rayleigh waves illuminate the medium. Shorter wavelengths are mainly influenced by the surficial partially saturated zone, where capillary suction plays a major role, while longer wavelengths spread most of their energy into deeper saturated regions. This is why surface-wave dispersion curves computed from the proposed model, which accounts for capillary suction effects, can be sensitive to remarkably small variations in water saturation. This characteristic makes the proposed model particularly interesting for extracting hydraulic information from passive seismic interferometry (e.g., Fores et al., 2018; Lecocq et al., 2017; Mordret et al., 2020), which is a newly emerging and promising field in hydrogeophysics. It is worth noting that interferometry studies generally do not consider ballistic waves (P, S, and surface waves as presented in this work) but use coda waves, which arise from locally scattered energy (Snieder, 2006). Saturation changes in the shallow subsurface would lead to velocity perturbations and as coda waves are primarily sensitive to the S-wave velocity (Aki & Chouet, 1975), models accounting for capillary suction effects might help to better characterize the vadose zone surrounding the recording stations. In addition, recent developments also suggest to exploit ballistic waves in seismic noise monitoring experiments, for instance, to track local water table variations (Garambois et al., 2019) or to perform seismic monitoring of very shallow infiltration tests (Hanafy et al., 2021) by combining active and passive methods. The model proposed here is of interest to such studies since it may help to better interpret observed velocity variations.

It is important to remark that the capillary-pressure-saturation relationship (Equation 14) constitutes a key element of the proposed model for exploring the vadose zone. The van Genuchten (1980) parameters, that is, S_{wr}, α_{vg}, and n_{vg}, are associated with specific values for each soil texture and also determine the impact that capillary suction effects have on the mechanical properties of the soil.

We can illustrate the effects of the van Genuchten (1980) parameters by varying each one of these parameters, within the proposed model, between maximum and minimum characteristic values provided by Carsel and Parrish (1988) for typical soil textures (Figure 7). The remaining parameter values are identical to the case studied in Figure 4. Interestingly, surface waves are not equally sensitive to the variations in S_{wr}, α_{vg}, and n_{vg}. Surface-wave

dispersion curves display a low sensitivity to changes in S_{wr} of the medium, showing maximum relative velocity variations of 1% for frequencies below 100 Hz and for residual saturation changing between $S_{wr}^{min} = 0.07$ and $S_{wr}^{max} = 0.26$ (Figure 7a). On the other hand, for the same frequencies, we observe that the effects of varying α_{vg} have a relatively small impact on the surface-wave dispersion curves, showing maximum relative velocity variations of -6% for values ranging between $\alpha_{wr}^{min} = 1\ m^{-1}$ and $\alpha_{wr}^{max} = 10\ m^{-1}$ (Figure 7b). Finally, the effects of varying the pore size distribution index n_{vg} between $n_{vg}^{min} = 1.1$ and $n_{vg}^{max} = 2.5$, for which relative variations of up to -37% prevail (Figure 7c). By comparing Figure 7c with Figure 4h, we note that when n_{vg} approaches n_{vg}^{max} (Figure 7c), dispersion curves approach the shape depicted by the rock physics model disregarding capillary suction (see red-dashed line in Figure 4h). This is an interesting feature, which further indicates that surface-wave dispersion curves in coarse-grained soil textures, which are associated with relatively large n_{vg} values, are not expected to be as sensitive to capillary effects as fine-grained soils, which, in turn, depict small n_{vg} values. Furthermore, this analysis shows that the proposed model has potential to provide valuable information, as far as static conditions are considered, with regard to α_{vg} and n_{vg}, while it appears relatively insensitive to S_{wr}.

Several key issues have yet to be resolved, both theoretically and numerically, to successfully invert surface-wave dispersion data using the proposed approach. First, the influence of the HM parameters such as N or f on materials and saturations has to be explored. As previously mentioned, these parameters may be stress dependent (e.g., Makse et al., 1999). Moreover, the influence of possible wave-induced fluid flow (WIFF) processes has to be addressed as soon as real data applications will be targeted (e.g., Milani et al., 2015), as the Biot-Gassmann-Wood low-frequency approximation may indeed fail, for instance, in the presence of patchy saturation (e.g., Solazzi et al., 2019). In this sense, the relative importance of different sources of attenuation and velocity dispersion in the data needs to be assessed, which is not a simple task. Future studies should also complement the current study by using the dynamic Richards (1931) equation to explore drainage-imbibition processes, accounting for the corresponding hysteresis in time-lapse measurements. In this context, it is important to recall that our calculations do not account for evapotranspiration processes and the presence of roots, which might induce strong water content variations in the vadose zone (e.g., Fisher, 2014). In addition, evapotranspiration processes can make the state of saturation diverge from the funicular regime toward the pendular regime. Water flow induced by evapotranspiration processes can be accounted for when solving the Richards equation (e.g., Voytek et al., 2019). Finally, analyzing surface-wave dispersion characteristics for higher modes as well as considering more complex layered media, involving vertical variations in texture and hydraulic properties, should provide further insights with regard to the nature and importance of capillary effects.

5. Conclusions

In this work, we study the effects of capillary suction on surface-wave dispersion curves. For this, we employ (a) a model describing both P- and S-wave velocities in unconsolidated and partially saturated granular media, which accounts for capillary effects and is consistent with experimental data; (b) saturation-depth profiles obtained by solving the static Richards equation describing two-phase flow; and (c) numerical algorithms that allow us to obtain surface-wave velocity dispersion and body-wave travel times in layered media. The numerical analyses shows that, for homogeneous granular media affected by overburden stress and the presence of a water table, body-wave travel times and Poisson's ratios computed using the proposed model show negligible differences when compared to models that disregard capillary suction effects. Conversely, when the water content in the vadose zone changes, accounting for capillary suction effects is necessary to explain the observed variations surface-wave dispersion. The general characteristics predicted by the proposed model in surface-wave dispersion curves when considering capillary effects were previously observed by other researchers in field measurements. Our results illustrate that these surface-wave velocity variations with the saturation-depth profile are predominant for medium-to fine-grained soils, which points to the importance of the soil texture on the water content in the vadose zone. In particular, the pore size distribution index plays a predominant role in this regard. The results of this study indicate that capillary suction should be considered to allow for an adequate interpretation of surface waves, offering a novel geophysical perspective for constraining soil water characteristics through seismic measurements.

Data Availability Statement

The data associated with this paper are available online from https://doi.org/10.5281/zenodo.5266459.

Acknowledgments
Damien Jougnot and Ludovic Bodet thank the support of the GeoProcesS project funded by the Emergence(s) Ville de Paris program as well as the CRITEX ANR-11-EQPX-0011 project. Santiago G. Solazzi and Klaus Holliger acknowledge partial support of the Swiss National Science Foundation (grant #200020−178946).

References

Aki, K., & Chouet, B. (1975). Origin of coda waves: Source, attenuation, and scattering effects. *Journal of Geophysical Research*, *80*(23), 3322–3342. https://doi.org/10.1029/jb080i023p03322

Bachrach, R., & Avseth, P. (2008). Rock physics modeling of unconsolidated sands: Accounting for nonuniform contacts and heterogeneous stress fields in the effective media approximation with applications to hydrocarbon exploration. *Geophysics*, *73*(6), E197–E209. https://doi.org/10.1190/1.2985821

Bachrach, R., Dvorkin, J., & Nur, A. (1998). High-resolution shallow-seismic experiments in sand, Part II: Velocities in shallow unconsolidated sand. *Geophysics*, *63*(4), 1234–1240. https://doi.org/10.1190/1.1444424

Bachrach, R., Dvorkin, J., & Nur, A. (2000). Seismic velocities and Poisson's ratio of shallow unconsolidated sands. *Geophysics*, *65*(2), 559–564. https://doi.org/10.1190/1.1444751

Bergamo, P., Bodet, L., Socco, L. V., Mourgues, R., & Tournat, V. (2014). Physical modelling of a surface-wave survey over a laterally varying granular medium with property contrasts and velocity gradients. *Geophysical Journal International*, *197*(1), 233–247. https://doi.org/10.1093/gji/ggt521

Bergamo, P., Dashwood, B., Uhlemann, S., Swift, R., Chambers, J., Gunn, D., & Donohue, S. (2016a). Time-lapse monitoring of climate effects on earthworks using surface waves. *Geophysics*, *81*(2). EN1–EN15. https://doi.org/10.1190/geo2015-0275.1

Bergamo, P., Dashwood, B., Uhlemann, S., Swift, R., Chambers, J. E., Gunn, D. A., & Donohue, S. (2016b). Time-lapse monitoring of fluid-induced geophysical property variations within an unstable earthwork using P-wave refraction. *Geophysics*, *81*(4), EN17–EN27. https://doi.org/10.1190/geo2015-0276.1

Bergamo, P., & Socco, L. (2016). P- and S-wave velocity models of shallow dry sand formations from surface wave multimodal inversion. *Geophysics*, *81*(4), R197–R209. https://doi.org/10.1190/geo2015-0542.1

Berryman, J. G. (1999). Origin of gassmann's equations. *Geophysics*, *64*(5), 1627–1629. https://doi.org/10.1190/1.1444667

Binley, A., Hubbard, S. S., Huisman, J. A., Revil, A., Robinson, D. A., Singha, K., & Slater, L. D. (2015). The emergence of hydrogeophysics for improved understanding of subsurface processes over multiple scales. *Water Resource Research*, *51*(6), 3837–3866. https://doi.org/10.1002/2015wr017016

Bishop, A. W., & Blight, G. (1963). Some aspects of effective stress in saturated and partly saturated soils. *Géotechnique*, *13*(3), 177–197. https://doi.org/10.1680/geot.1963.13.3.177

Blazevic, L. A., Bodet, L., Pasquet, S., Linde, N., Jougnot, D., & Longuevergne, L. (2020). Time-lapse seismic and electrical monitoring of the vadose zone during a controlled infiltration experiment at the Ploemeur hydrological observatory, France. *Water*, *12*(5), 1230. https://doi.org/10.3390/w12051230

Bodet, L. (2019). *Surface waves modelling and analysis in media of increasing degrees of complexity (Habilitation à diriger des recherches, Sorbonne Université)*. Retrieved from https://hal.sorbonne-universite.fr/tel-02866882

Bodet, L., Dhemaied, A., Martin, R., Mourgues, R., Rejiba, F., & Tournat, V. (2014). Small-scale physical modeling of seismic-wave propagation using unconsolidated granular media. *Geophysics*, *79*(6), T323–T339. https://doi.org/10.1190/geo2014-0129.1

Bradford, J. H., & Sawyer, D. S. (2002). Depth characterization of shallow aquifers with seismic reflection, Part II—Prestack depth migration and field examples. *Geophysics*, *67*(1), 98–109. https://doi.org/10.1190/1.1451372

Carsel, R. F., & Parrish, R. S. (1988). Developing joint probability distributions of soil water retention characteristics. *Water Resource Research*, *24*(5), 755–769. https://doi.org/10.1029/wr024i005p00755

Cho, G., & Santamarina, J. (2001). Unsaturated particulate materials—Particle-level studies. *Journal of Geotechnical and Geoenvironmental Engineering*, *127*(1), 841. https://doi.org/10.1061/(asce)1090-0241(2001)127:1(84)

Dangeard, M., Bodet, L., Pasquet, S., Thiesson, J., Guérin, R., Jougnot, D., & Longuevergne, L. (2018). Estimating picking errors in near-surface seismic data to enable their time-lapse interpretation of hydrosystems. *Near Surface Geophysics*, *16*(6), 613–625. https://doi.org/10.1002/nsg.12019

Dong, Y., & Lu, N. (2016). Dependencies of shear wave velocity and shear modulus of soil on saturation. *Journal of Engineering Mechanics*, *142*(11), 04016083. https://doi.org/10.1061/(asce)em.1943-7889.0001147

Dvorkin, J., Prasad, M., Sakai, A., & Lavoie, D. (1999). Elasticity of marine sediments: Rock physics modeling. *Geophysical Research Letters*, *26*(12), 1781–1784. https://doi.org/10.1029/1999gl900332

Fisher, J. B. (2014). Land-atmosphere interactions, evapotranspiration. In E. G. Njoku (Ed.), *Encyclopedia of remote sensing* (pp. 325–328). Springer New York. https://doi.org/10.1007/978-0-387-36699-9_82

Fores, B., Champollion, C., Mainsant, G., Albaric, J., & Fort, A. (2018). Monitoring saturation changes with ambient seismic noise and gravimetry in a karst environment. *Vadose Zone Journal*, *17*, 170163. https://doi.org/10.2136/vzj2017.09.0163

Foti, S., Hollender, F., Garofalo, F., Albarello, D., Asten, M., Bard, P.-Y., et al. (2018). Guidelines for the good practice of surface wave analysis: A product of the interpacific project. *Bulletin of Earthquake Engineering*, *16*(6), 2367–2420. https://doi.org/10.1007/s10518-017-0206-7

Fratta, D., Alshibli, K. A., Tanner, W. M., & Roussel, L. (2005). Combined TDR and P-wave velocity measurements for the determination of in situ soil density—Experimental study. *Geotechnical Testing Journal*, *28*(6), 553–563.

Friedman, S. P. (2005). Soil properties influencing apparent electrical conductivity: A review. *Computers and Electronics in Agriculture*, *46*(1–3), 45–70. https://doi.org/10.1016/j.compag.2004.11.001

Gabriels, P., Snieder, R., & Nolet, G. (1987). In situ measurements of shear-wave velocity in sediments with higher-mode Rayleigh waves. *Geophysical Prospecting*, *35*(2), 187–196. https://doi.org/10.1111/j.1365-2478.1987.tb00812.x

Garambois, S., Voisin, C., Romero Guzman, M., Brito, D., Guillier, B., & Réfloch, A. (2019). Analysis of ballistic waves in seismic noise monitoring of water table variations in a water field site: Added value from numerical modelling to data understanding. *Geophysical Journal International*, *219*(3), 1636–1647. https://doi.org/10.1093/gji/ggz391

García, X., & Medina, E. A. (2006). Hysteresis effects studied by numerical simulations: Cyclic loading-unloading of a realistic sand model. *Geophysics*, *71*(2), F13–F20. https://doi.org/10.1190/1.2181309

Gassmann, F. (1951). Über die Elastizität poröser Medien. *Vierteljahrsschrift der naturforschenden Gesellschaft in Zürich*, *96*, 1–23.

Grelle, G., & Guadagno, F. M. (2009). Seismic refraction methodology for groundwater level determination: "Water seismic index". *Journal of Applied Geophysics*, *68*(3), 301–320. https://doi.org/10.1016/j.jappgeo.2009.02.001

Guarracino, L. (2007). Estimation of saturated hydraulic conductivity k_s from the van genuchten shape parameter α. *Water Resource Research*, *43*(11). https://doi.org/10.1029/2006wr005766

Hanafy, S. M., Hoteit, H., Li, J., & Schuster, G. T. (2021). Near-surface real-time seismic imaging using parsimonious interferometry. *Scientific Reports*, *11*(1), 1–9. https://doi.org/10.1038/s41598-021-86531-5

Haskell, N. A. (1953). The dispersion of surface waves on multilayered media. *Bulletin of the Seismological Society of America*, *43*, 17–34. https://doi.org/10.1785/bssa0430010017

Heitor, A., Indraratna, B., Rujikiatkamjorn, C., & Golaszewski, R. (2012). Characterising compacted fills at penrith lakes development site using shear wave velocity and matric suction. In *11th Australia - New Zealand conference on geomechanics: Ground engineering in a changing world* (pp. 1262–1267).

Herrmann, R. B. (2013). Computer programs in seismology: An evolving tool for instruction and research. *Seismological Research Letters*, *84*(6), 1081–1088. https://doi.org/10.1785/0220110096

Hill, R. (1952). The elastic behaviour of a crystalline aggregate. *Proceedings of the Physical Society Section A*, *65*(5), 349–354. https://doi.org/10.1088/0370-1298/65/5/307

Hornbaker, D., Albert, R., Albert, I., Barabási, A.-L., & Schiffer, P. (1997). What keeps sandcastles standing? *Nature*, *387*(6635), 765. https://doi.org/10.1038/42831

Hubbard, S. S., & Linde, N. (2011). Hydrogeophysics. In P. Wilderer (Ed.), *Treatise on water science* (Vol. 1, pp. 401–434). Academic Press. https://doi.org/10.1016/b978-0-444-53199-5.00043-9

Konstantaki, L. A., Carpentier, S. F. A., Garofalo, F., Bergamo, P., & Socco, L. V. (2013). Determining hydrological and soil mechanical parameters from multichannel surface-wave analysis across the Alpine Fault at Inchbonnie, New Zealand. *Near Surface Geophysics*, *11*(4), 435–448. https://doi.org/10.3997/1873-0604.2013019

Lecocq, T., Longuevergne, L., Pedersen, H. A., Brenguier, F., & Stammler, K. (2017). Monitoring ground water storage at mesoscale using seismic noise: 30 years of continuous observation and thermo-elastic and hydrological modeling. *Scientific Reports*. https://doi.org/10.1038/s41598-017-14468-9

Lu, N., Godt, J. W., & Wu, D. T. (2010). A closed-form equation for effective stress in unsaturated soil. *Water Resour. Res.*, *46*(5). https://doi.org/10.1029/2009wr008646

Lu, N., & Likos, W. J. (2004). *Unsaturated soil mechanics*. Wiley.

Lu, N., & Likos, W. J. (2006). Suction stress characteristic curve for unsaturated soil. *Journal of Geotechnical and Geoenvironmental Engineering*, *132*(2), 131–142. https://doi.org/10.1061/(asce)1090-0241(2006)132:2(131)

Lu, Z. (2014). Feasibility of using a seismic surface wave method to study seasonal and weather effects on shallow surface soils. *Journal of Environmental & Engineering Geophysics*, *19*(2), 71–85. https://doi.org/10.2113/jeeg19.2.71

Lu, Z., & Sabatier, J. M. (2009). Effects of soil water potential and moisture content on sound speed. *Soil Science Society of America Journal*, *73*(5), 1614–1625. https://doi.org/10.2136/sssaj2008.0073

Makse, H. A., Gland, N., Johnson, D. L., & Schwartz, L. M. (1999). Why effective medium theory fails in granular materials. *Physical Review Letters*, *83*(24). https://doi.org/10.1103/physrevlett.83.5070

Mavko, G., Mukerji, T., & Dvorkin, J. (2020). *The rock physics handbook*. Cambridge university press.

Milani, M., Rubino, J. G., Baron, L., Sidler, R., & Holliger, K. (2015). Attenuation of sonic waves in water-saturated alluvial sediments due to wave-induced fluid flow at microscopic, mesoscopic and macroscopic scales. *Geophysical Journal International*, *203*(1), 146–157. https://doi.org/10.1093/gji/ggv287

Mindlin, R. D. (1949). Compliance of elastic bodies in contact. *Journal of Applied Mechanics, ASME*, *16*, 259–268. https://doi.org/10.1115/1.4009973

Mordret, A., Courbis, R., Brenguier, F., Chmiel, M., Garambois, S., Mao, S., et al. (2020). Noise-based ballistic wave passive seismic monitoring–part 2: Surface waves. *Geophysical Journal International*, *221*(1), 692–705. https://doi.org/10.1093/gji/ggaa016

Murphy, W. F. (1982). *Effects of microstructure and pore fluids on the acoustic properties of granular sedimentary materials*. Ph. D. dissertation, Stanford University.

Nuth, M., & Laloui, L. (2008). Effective stress concept in unsaturated soils: Clarification and validation of a unified framework. *International Journal for Numerical and Analytical Methods in Geomechanics*, *32*(7), 771–801. https://doi.org/10.1002/nag.645

Parsekian, A., Singha, K., Minsley, B. J., Holbrook, W. S., & Slater, L. (2015). Multiscale geophysical imaging of the critical zone. *Reviews of Geophysics*, *53*(1), 1–26. https://doi.org/10.1002/2014rg000465

Pasquet, S., & Bodet, L. (2017). SWIP: An integrated workflow for surface-wave dispersion inversion and profiling. *Geophysics*, *82*(6), WB47–WB61. https://doi.org/10.1190/geo2016-0625.1

Pasquet, S., Bodet, L., Bergamo, P., Guérin, R., Martin, R., Mourgues, R., & Tournat, V. (2016a). Small-scale seismic monitoring of varying water levels in granular media. *Vadose Zone Journal*, *15*(7), vzj2015.11.0142. https://doi.org/10.2136/vzj2015.11.0142

Pasquet, S., Bodet, L., Dhemaied, A., Mouhri, A., Vitale, Q., Rejiba, F., et al. (2015a). Detecting different water table levels in a shallow aquifer with combined P-, surface and SH-wave surveys: Insights from V_p/V_s or Poisson's ratios. *Journal of Applied Geophysics*, *113*, 38–50. https://doi.org/10.1016/j.jappgeo.2014.12.005

Pasquet, S., Bodet, L., Longuevergne, L., Dhemaied, A., Camerlynck, C., Rejiba, F., & Guérin, R. (2015b). 2D characterization of near-surface V_p/V_s: Surface-wave dispersion inversion versus refraction tomography. *Near Surface Geophysics*, *13*(4), 315–332. https://doi.org/10.3997/1873-0604.2015028

Pasquet, S., Holbrook, W. S., Carr, B. J., & Sims, K. W. W. (2016b). Geophysical imaging of shallow degassing in a Yellowstone hydrothermal system. *Geophysical Research Letters*, *43*(23), 2016GL071306. https://doi.org/10.1002/2016GL071306

Pride, S. R. (2005). Relationships between seismic and hydrological properties. In Y. Rubin, & S. Hubbard (Eds.), *Hydrogeophysics* (pp. 253–290). Springer.

Richards, L. A. (1931). Capillary conduction of liquids through porous mediums. *Physics*, *1*(5), 318–333. https://doi.org/10.1063/1.1745010

Romero-Ruiz, A., Linde, N., Baron, L., Solazzi, S. G., Keller, T., & Or, D. (2021). Seismic signatures reveal persistence of soil compaction. *Vadose Zone Journal*, *20*(4), e20140.

Rubin, Y., & Hubbard, S. S. (2006). *Hydrogeophysics* (Vol. 50). Springer Science & Business Media.

Santamarina, J., Rinaldi, V., Fratta, D., Klein, K., Wang, Y., Cho, G., & Cascante, G. (2005). A survey of elastic and electromagnetic properties of near-surface soils. In *Near-surface geophysics* (pp. 71–88). Society of Exploration Geophysicists. https://doi.org/10.1190/1.9781560801719.ch4

Sawangsuriya, A., Edil, T. B., & Bosscher, P. J. (2009). Modulus-suction-moisture relationship for compacted soils in postcompaction state. *Journal of Geotechnical and Geoenvironmental Engineering*, *135*(10), 1390–1403. https://doi.org/10.1061/(asce)gt.1943-5606.0000108

Shearer, P. M. (2019). *Introduction to seismology*. Cambridge university press.

Shen, J., Crane, J. M., Lorenzo, J. M., & White, C. D. (2016). Seismic velocity prediction in shallow (<30 m) partially saturated, unconsolidated sediments using effective medium theory. *Journal of Environmental & Engineering Geophysics*, *21*(2), 67–78. https://doi.org/10.2113/jeeg21.2.67

Shen, J., Lorenzo, J. M., White, C. D., & Tsai, F. (2015). Soil density, elasticity, and the soil-water characteristic curve inverted from field-based seismic P-and S-wave velocity in shallow nearly saturated layered soils. *Geophysics*, *80*(3), WB11–WB19. https://doi.org/10.1190/geo2014-0119.1

Snieder, R. (2006). The theory of coda wave interferometry. *Pure and Applied Geophysics*, *163*(2), 455–473. https://doi.org/10.1007/s00024-005-0026-6

Socco, L. V., & Strobbia, C. (2004). Surface-wave method for near surface characterization: A tutorial. *Near Surface Geophysics*, *2*(4), 165–185. https://doi.org/10.3997/1873-0604.2004015

Solazzi, S. G., Guarracino, L., Rubino, J. G., & Holliger, K. (2019). Saturation hysteresis effects on the seismic signatures of partially saturated heterogeneous porous rocks. *Journal of Geophysical Research: Solid Earth*, *124*(11), 11316–11335. https://doi.org/10.1029/2019jb017726

Suzaki, A., Minato, S., Ghose, R., Konishi, C., & Sakai, N. (2017). Modelling time-lapse shear-wave velocity changes in an unsaturated soil embankment due to water infiltration and drainage. *First Break*, *35*(8), 81–90. https://doi.org/10.3997/1365-2397.35.8.89811

Terzaghi, K. V. (1923). Die Berechnung der Durchassigkeitsziffer des Tones aus dem Verlauf der hydrodynamischen Spannungs. *Mathemat-ish-Naturwissen-Schaftiliche Klasse*, *132*, 105–124.

Thomson, W. T. (1950). Transmission of elastic waves through a stratified solid medium. *Journal of Applied Physics*, *21*(2), 89–93. https://doi.org/10.1063/1.1699629

Turesson, A. (2007). A comparison of methods for the analysis of compressional, shear, and surface wave seismic data, and determination of the shear modulus. *Journal of Applied Geophysics*, *61*(2), 83–91. https://doi.org/10.1016/j.jappgeo.2006.04.005

van Genuchten, M. T. (1980). A closed-form equation for predicting the hydraulic conductivity fo unsaturated soils. *Soil Science Society of America Journal*, *44*, 892–898. https://doi.org/10.2136/sssaj1980.03615995004400050002x

Voytek, E. B., Barnard, H. R., Jougnot, D., & Singha, K. (2019). Transpiration-and precipitation-induced subsurface water flow observed using the self-potential method. *Hydrological Processes*, *33*(13), 1784–1801.

Vriend, N. M., Hunt, M. L., Clayton, R. W., Brennen, C. E., Brantley, K. S., & Ruiz-Angulo, A. (2007). Solving the mystery of booming sand dunes. *Geophysical Research Letters*, *34*, L16306. https://doi.org/10.1029/2007gl030276

West, M., & Menke, W. (2000). Fluid-induced changes in shear velocity from surface waves. In *Symposium on the application of geophysics to engineering and environmental problems* (pp. 21–28). https://doi.org/10.3997/2214-4609-pdb.200.2000_003

Zyserman, F. I., Monachesi, L. B., & Jouniaux, L. (2017). Dependence of shear wave seismoelectrics on soil textures: A numerical study in the vadose zone. *Geophysical Journal International*, *208*(2), 918–935. https://doi.org/10.1093/gji/ggw431